Report R88-920030-F

PROPULSOR BLADE FLOWS

T.R. Govindan, R. Levy, W.R. Briley, and S.J. Shamroth
Scientific Research Associates, Inc.
Glastonbury, CT 06033

Final Report
Contract N00014-86-C-0166

*Original contains color plates: All DTIC reproductions will be in black and white.

Prepared for:
Office of Naval Research
Department of the Navy
Arlington, VA 22217-5000

December 1988

I. INTRODUCTION

The performance characteristics of a hydrodynamic propulsor are determined, to a large extent, by complex three-dimensional viscous flow in the blade rows. The capability to compute the complex flow field for use in the design and analysis of performance of a propulsor would be a valuable tool for improving performance.

Research under the present contract addressed computation of the steady flow field in shrouded propulsor blade rows. A prime consideration in the choice of a computation procedure is the multiplicity of length scales in the shrouded propulsor flow field that need to be adequately resolved. The differing dominant flow mechanisms at the hub and tip of the blade, blade boundary layers, and a core inviscid flow characterize the multiple length scales. A single computation procedure, useful in a design and analysis context, that adequately resolved all of the flow length scales was deemed uneconomical due to the large number of grid points that would be necessary for the computation. The approach pursued, under the present contract, was to study the flow field in the tip and hub regions of the blade in separate more tractable computations (zonal approach).

The dominant flow mechanisms in the blade tip region of a shrouded propulsor are due to tip clearance effects and the shroud boundary layer. A preliminary analysis of the physics of the shrouded propulsor tip flow field indicated that a unique spatial-marching procedure developed at SRA could be utilized to compute this flow field. The primary motivation in adopting this approach was the very high density grids required for adequate resolution of the complex flow structure of the shrouded tip flow field. Spatial-marching procedures can utilize these high density grids far more economically than methods for the three-dimensional Navier-Stokes equations. The accuracy and high computational efficiency of the spatial-marching analysis has been demonstrated in applications to internal and external flows [1-4]. The run time needed for solution is 10 to 100 times less than that required for the Navier-Stokes equations. Success of the proposed approach could provide the capability to address a very difficult viscous flow problem with both economy and accuracy.

The approximate flow equations solved in the spatial-marching procedure were judged to be inadequate for the hub region of the propulsor flow field.

This is due to the fact that the approximations made are inaccurate in the region of the blunt leading edge of the propulsor blade at the hub. Furthermore, the hub flow field often contains a large region of separated flow at the corner of the suction surface of the blade and the hub. Large regions of streamwise flow separation are beyond the scope of the spatial-marching procedure. Solution of the Navier-Stokes equations was proposed for the propulsor hub flow field.

The present report describes progress made under the Propulsor Blade Flows contract towards computations of the tip and hub flow fields of a shrouded propulsor. The next section of the report describes the application of the spatial-marching procedure to the shrouded propulsor blade tip flow field. The third section of the report describes progress towards application of a Navier-Stokes solution procedure to the hub flow field.

2. SHROUDED PROPULSOR BLADE TIP FLOW FIELD

An analysis of the application of the spatial-marching procedure to the shrouded tip flow field was carried out for the purpose of defining approximations and boundary conditions. Such an analysis also provided insight into the physical nature of the flow field in the region of the shrouded tip. A model problem was devised for this purpose and consisted of a constant thickness blade with a square tip and a moving shroud wall (Figure A). The moving shroud wall simulates relative motion between the propulsor blade tip and the shroud. This simplified problem geometry was chosen to focus efforts on key elements of the shrouded tip flow structure affected by the physical approximations made in the primary/secondary flow equations solved by spatial-marching.

A critical aspect of computing the shrouded tip flow field and the flow field of the model problem is the mass flux through the tip clearance region. This mass flux is controlled, to a large extent, by transverse and streamwise pressure gradients in the tip clearance region, viscous effects of the relative motion between the shroud and the blade tip, and the mass flux through the lateral boundaries of the computational domain. Approximating streamwise pressure gradients as a means to obtain equations that are well-posed for spatial-marching was judged to be inappropriate as a physical approximation due to the strong influence of this pressure gradient on the computed mass flux

through the tip clearance. Typically, approximate streamwise pressure gradients are obtained from the potential flow through the geometry under consideration. For the model problem the potential flow streamwise pressure gradient is zero. Computations for the model problem with the streamwise pressure gradient set to zero produced non-physical flow fields.

Generalized primary/secondary flow equations have been derived at SRA [1, 2], well-posed for a spatial-marching procedure, that introduce no approximations for pressure gradients. Approximations are introduced, instead, on the scalar potential component of a decomposed transverse velocity field. The scalar potential velocity component is defined to be normal to a local primary flow direction. Typically, the primary flow direction is chosen to be the direction of the potential flow streamline at the point. Appendix I describes the generalized primary/secondary flow equations and a sequentially decoupled implicit algorithm used to solve the equations.

Application of the generalized primary/secondary flow equations to the shrouded tip flow field required integrating the spatial-marching procedure with the treatment of the blade tip region as a local zone. The model problem (Figure A) provided a simple geometry to test developed procedures. A key element in this development was to construct appropriate boundary conditions at lateral boundaries for the generalized primary/secondary flow equations. Accuracy of the approach could be judged by the magnitude of the computed scalar potential velocities in the flow field. Boundary conditions along the other boundaries of the model problem have been developed in previous work or were straightforward. Boundary conditions on the shroud and blade surfaces were derived from the no-slip condition on a solid surface. Inboard boundary conditions have been developed for the tip vortex flow field [3] and are suitable for the shrouded tip flow field. However, for the preliminary computations carried out, the flow field was assumed to be symmetric along the inboard boundary. These boundary conditions simplified the development and testing of lateral boundary conditions appropriate for the zonal approach.

Two approaches were attempted in the development of lateral boundary conditions for the primary/secondary flow equations along with the zonal approach. These conditions needed to be specified in terms of the scalar and vector potentials for the decomposed transverse velocity field. The critical element in these conditions is the value of the vector potential on the shroud that represents the mass flux entrained by the relative motion between the

blade tip and the shroud. The first approach determined the value of the vector potential on the shroud from a local boundary layer analysis at the lateral boundary. However, computations for the model problem showed large scalar potential velocities and, therefore, inaccurate solutions. Small errors in mass flux, due to the approximate boundary layer analysis, at the lateral boundary were magnified at the small tip clearance gap. The second approach attempted a local analysis in the clearance gap, based on small normal velocites in the gap, to determine the vector potential on the shroud. The second approach was also unsuccessful due to inaccurate solutions from a large scalar potential velocity field.

All of the lateral boundary conditions developed and tested in the present investigation led to large scalar potential velocities near the tip clearance gap. Consequently, the physical approximations required to effect a spatial-marching solution were inaccurate for this flow application. From these results the conclusion was reached that considerable further work and analysis for lateral boundary conditions would be required before attempting a zonal approach together with the spatial-marching procedure for computing the shrouded tip flow field.

3. A COORDINATE SYSTEM FOR THE NAVIER-STOKES CALCULATION OF A PROPELLER HUB FLOW FIELD

A coordinate sytem is one component in the application of finite-difference numerical techniques to fluid dynamics problems. A good coordinate system should minimize the error in the governing equations for the problem being analyzed. Failure to adequately resolve changes in the fluid dynamic properties between mesh points is one source of error. Excessive changes in grid spacing between neighboring grid points as well as excessive coordinate curvature and non-orthogonality also produce error terms. An accurate calculation requires a coordinate system with adequate resolution of the gradients of the flow variables and smoothness of the computational grid.

In generating the propeller hub coordinate system, care has been taken to resolve near wall regions and to provide smoothness of the grid lines and of the grid spacing along each line. This is accomplished by building a three-dimensional coordinate system from a series of well-behaved two-dimensional coordinate systems. The two-dimensional coordinates are

generated to have favorable smoothness properties and the subsequent mappings are designed to preserve the favorable smoothness properties of the coordinates.

An H-type coordinate system about an uncambered Joukowski airfoil is generated using potential lines and streamlines about the airfoil at zero incidence. The streamlines are mapped to horizontal lines at a specific distance from the airfoil. This coordinate system is shown in Figure 1a. A series of these airfoils can be stacked to form a cascade of zero pitch. This coordinate system provides nearly orthogonal coordinates and fine resolution near the blades, as shown in Figure 1b. Grid clustering is provided in the streamwise direction near the leading and trailing edges. Stacking this coordinate system provides continuity of location, slope and curvature for the vertical coordinate lines across the upper and lower boundaries.

Pitch is added to the cascade by performing a shearing transformation shown in Figure 2. The shearing transformation produces a midline shape of a circular arc with upstream and downstream straight line extensions. The circular arc need not coincide with the blade chord. The inflow and outflow boundaries are straight vertical lines. The shearing transformation distorted the blade shapes and, since Joukowski thickness distributions are not used in practice, the desired blade thickness distribution is imposed. A blade thickness distribution is imposed normal to the midline of the sheared blade. The coordinate lines emanating from the blade are relaxed to the new blade surface. The results of this process is shown in Figure 2 for a blade thickness distribution

$$\frac{Y}{C} = \pm 0.15 \left(\sqrt{\frac{X}{C}} - \frac{X}{C} \right) \qquad (1)$$

where X is the distance along the chord, Y is the distance from the chord to the blade and C is the chord length.

This coordinate system can be stacked to form a cascade of airfoils as shown in Figure 3. At the upper and lower boundaries the coordinates are continuous in location, slope and curvature making application of periodic boundary conditions very natural. In addition, the coordinates are clustered vertically near the blades and horizontally near the leading and trailing edges to ensure resolution of the large gradients of the flow.

Specifying blade shape and coordinate system length and width, coordinate systems such as shown in Figure 2 are mapped into θ,z surfaces in the hub coordinate system. Note that in these surfaces the radius will be a function of the z coordinate as shown in the side view of the hub in Figure 4. These r,z coordinates are computed as the leading edge of a thick airfoil (turned backwards) using potential lines and streamlines as outlined above.

The x,y coordinates of Figure 2 are mapped into the r,z surfaces of Figure 4. Figure 5 shows three blades on a hub with the r,z coordinate lines of Figure 4 shown in white. Figure 6 shows the inner and outer θ,z surfaces. These blades are stacked on their leading edges, although the choice of stacking location can be specified. Blade twist is seen from the twist of the upstream extension of the coordinate system. Five regions of fine resolution are contained in this coordinate system: 1) hub surface, 2) hub trailing edge, 3) blade surfaces, 4) blade leading edge and 5) blade trailing edge.

CONCLUSIONS

(a) Application of a spatial-marching procedure to compute the shrouded tip flow field was unsuccessful due to the inability to construct boundary conditions compatible with the approximations in the flow equations.

(b) A grid generation procedure for the propulsor hub flow field to construct computational grids for use with a Navier-Stokes solver was successfully completed.

Appendix I

1. Background

The primary/secondary flow equations derived in Ref. 1 are an approximate set of flow equations suitable for complex three-dimensional flow problems with a dominant flow direction that could contain large streamwise vorticity. Streamwise viscous diffusion is small in such flows, compared to transverse diffusion, and is neglected in the primary/secondary flow equations. The small scalar potential approximation makes the primary/secondary flow equations a well-posed initial-value problem in the streamwise coordinate direction. The streamwise coordinate is nominally aligned with the dominant flow direction. An important element in the derivation of the primary/secondary flow equations is that the approximations are associated with directions identified by a vector basis at each point in the flow field, distinct from coordinate directions. The vector basis for the approximations provides considerable flexibility in choosing convenient coordinate systems for complex three-dimensional geometries, while at the same time making valid flow approximations.

The motivation in deriving the primary/secondary flow equations is to obtain a set of approximate equations that can be solved economically compared to solving the full Navier-Stokes equations. The primary/secondary flow equations can be solved as an initial-value problem in the streamwise coordinate direction, compared to the boundary-value Navier-Stokes equations in the same direction, with potential savings in computational effort and storage requirements. These savings provide the ability to solve a large number of flow cases, with sufficient grid points to resolve complex three-dimensional flow fields, from limited resources. An algorithm is developed to solve the primary/secondary equations that provides an order of magnitude (factor of 10 to 20) advantage in computational effort over an efficient Navier-Stokes solver.

The next section of this Appendix contains a list of the primary/secondary flow equations derived in Ref. 1. Properties of the equations that affect the choice of the solution algorithm are discussed. A Sequentially Decoupled Implicit algorithm is developed as an efficient means of solving the primary/secondary equations. Numerical procedures that comprise the algorithm and their implementation are discussed.

2. Primary/Secondary Flow Equations

The primary/secondary flow equations are listed here for convenience of presenting the solution algorithm. Derivation of these equations can be found in Ref. 1. In the equations that follow, i_k denotes the unit vector basis associated with the orthogonal reference line coordinate system. The vector $\bar{i}_1$ is aligned with the reference line direction (x_1) along which the primary/secondary flow equations are an initial-value problem. The vector basis $\bar{e}_k$ and the reciprocal basis $\bar{e}^k$ are defined for the purpose of approximating flow equations.

$$\bar{e}_k \cdot \bar{e}^{\ell} = e_{km} e^{m\ell} = \delta_k^{\ell} \tag{2.1}$$

The flow field velocity vector is denoted by $\bar{U}$,

$$\bar{U} = u_1 \bar{i}_1 + u_2 \bar{i}_2 + u_3 \bar{i}_3 = u_p \bar{e}^1 + v\bar{e}^2 + w\bar{e}^3 \tag{2.2}$$

The velocity component u_p is associated with the primary flow direction and components v and w with the secondary flow field. The secondary flow velocity vector $\bar{V}$ can be defined as

$$\bar{V} = v\bar{e}^2 + w\bar{e}^3 \tag{2.3}$$

The secondary flow velocity components are decomposed into scalar potential (v_ϕ, w_ϕ) and vector potential components (v_ψ, w_ψ)

$$\begin{aligned} v &= v_\phi + v_\psi \\ w &= w_\phi + w_\psi \\ \bar{V} &= \bar{V}_\phi + \bar{V}_\psi \end{aligned} \tag{2.4}$$

The scalar potential velocity components can be defined in terms of a scalar potential (ϕ) and the vector potential components in terms of a vector potential (ψ).

$$\nabla_s\phi = (e^{\ell j}\bar{V}_\phi\cdot\bar{e}_j)\bar{i}_\ell$$

$$\ell = 2,3 \text{ (no sum)} \qquad (2.5)$$

$$\nabla_s\times\psi\bar{i}_1 = (\rho e^{\ell j}\bar{V}_\psi\cdot\bar{e}_j)\bar{i}_\ell$$

where ρ is density and ∇_s is the surface operator defined as

$$\nabla_s = \nabla - \nabla_p \qquad (2.6)$$

with $$\nabla_p = \bar{i}_1(\bar{i}_1\cdot\nabla)$$

All variables in the flow equations are assumed to be nondimensional, having been normalized by a suitable combination of reference quantities. The primary/secondary flow equations are written for the dependent variables, streamwise velocity u_p, scalar potential ϕ, vector potential ψ, vorticity Ω, pressure p, total enthalpy E, and density ρ.

Scalar potential equation (continuity):

$$\nabla_s\cdot(\rho\nabla_s\phi) + \nabla_p\cdot(\rho e^{1j}\bar{V}\cdot\bar{e}_j)\bar{i}_1 + \nabla\cdot(\rho e^{kl}u_p)\bar{i}_k = 0 \qquad (2.7)$$

Streamwise momentum equation:

$$\rho\bar{U}\cdot\nabla u_p - \rho\bar{U}\cdot(\bar{U}\cdot\nabla)\bar{e}_1 + \bar{e}_1\cdot\nabla p + \frac{1}{Re}\bar{e}_1\cdot\tilde{\nabla}\times\mu\tilde{\nabla}\times\bar{U} = 0 \qquad (2.8)$$

where Re is the Reynolds number defined from reference quantities, μ the normalized coefficient of molecular viscosity, and $\tilde{\nabla}$ is an approximation to ∇ in which second derivatives along the $\bar{i}_1$ coordinate have been neglected.

Vector potential equation (definition of vorticity):

$$\nabla_s\times\frac{1}{\rho}(\nabla_s\times\psi\bar{i}_1) - \Omega\bar{i}_1 = 0 \qquad (2.9)$$

Vorticity transport equation:

$$\frac{\rho u_p}{h}\frac{\partial \Omega}{\partial x_1} + \nabla_s\cdot\rho\bar{V}\Omega + \nabla_s\times(e^{\ell k}C_k - D^{\ell})\bar{i}_{\ell} + (\nabla_s\frac{\rho u_p}{h})\times\frac{\partial e^{\ell k}}{\partial x_1}(\bar{V}\cdot\bar{e}_k)\bar{i}_{\ell}$$

$$+ (\nabla_s\rho\bar{V})\times[\nabla_s e^{\ell k}(\bar{V}\cdot\bar{e}_k)]\bar{i}_{\ell} + \frac{1}{Re}\nabla_s\times e^{\ell k}\bar{e}_k\cdot\nabla_s\times\mu\Omega\bar{i}_1 = 0 \qquad (2.10)$$

where C_k and D^{ℓ} are defined in [1] and $\bar{V} = \beta\bar{V}_{\phi} + \bar{V}_{\psi}$. The parameter β takes on values of 0 or 1, $\beta = 0$ identifies the small scalar potential approximation.

Pressure equation:

$$\nabla_s\cdot(e^{\ell k}\bar{e}_k\cdot\nabla p)\bar{i}_{\ell} + \nabla_s\cdot(e^{\ell k}F_k)\bar{i}_{\ell} = 0 \quad \ell = 2,3 \quad \text{(no sum)} \qquad (2.11)$$

F_k is a combination of terms from transverse momentum equations and is defined in [1]. The secondary flow velocity vector, $\bar{V}$, is written as $\bar{V} = \beta\bar{V}_{\phi} + \bar{V}_{\psi}$ in F_k and $\beta = 0$ identifies the small scalar potential approximation.

Energy equation:

$$\rho\bar{U}\cdot\nabla E - (RePr)^{-1}\nabla\cdot\kappa\nabla_s E - (\gamma-1)M_r^2Re^{-1}[\mu\Phi - \rho\bar{U}\cdot\nabla_s\times\mu\nabla_s\times\bar{q}$$

$$- Pr^{-1}\nabla_s\kappa\nabla_s|\bar{q}|^2/2] = 0 \qquad (2.12)$$

where $\bar{q} = u_p\bar{e}^1 + (\beta v_{\phi} + v_{\psi})\bar{e}^2 + (\beta w_{\phi} + w_{\psi})\bar{e}^3$,

Φ is the dissipation function, κ the coefficient of thermal conductivity, Pr the Prandtl number, and M_r the reference Mach number. Simpler forms of the energy equation that can be used at low and moderate Mach numbers are described in [1].

State equation:

$$p = \rho E/\gamma M_r^2 - (\gamma-1)\rho|\bar{q}|^2/2\gamma \qquad (2.13)$$

Equations (2.7) to (2.13), along with the definition of the velocity decomposition (2.5), are the complete set of primary/secondary flow equations. The small scalar potential approximation ($\beta = 0$) makes these equations a well-posed initial value problem along the streamwise coordinate (x_1).

3. Solution of Primary/Secondary Flow Equations

The choice of a solution algorithm for the primary/secondary flow equations must exploit the small scalar potential approximation for economy. The potential for economy lies in the initial-value nature of the primary/secondary flow equations and the ability to solve such a problem by a spatial marching scheme. Such a scheme will be developed in this section for the primary/secondary flow equations.

An evolution equation can be written in the form

$$A \frac{\partial \phi}{\partial t} + D(\phi) = 0 \qquad (3.1)$$

where ϕ is a vector of dependent variables, t is a time-like variable (e.g. streamwise coordinate), A is a matrix of coefficients, and D is a multi-dimensional differential operator. Efficient, implicit, noniterative marching schemes have been developed to solve equations of the type (3.1) when the matrix A is well-conditioned. An example of such a scheme is the LBI scheme [5] for nonlinear equations and is based on the Douglas-Gunn ADI scheme. However, the matrix A for the primary/secondary flow equations is singular due to the lack of streamwise derivatives in some of the governing equations. This is also true when the same equations are written in terms of primitive variables [1]. Coupled implicit schemes such as the LBI scheme require iteration when A is singular. This penalty in economy, due to iteration of a fully coupled system at each step, is avoided in the present sequentially decoupled algorithm.

The problem with the singularity of the coefficient matrix of the streamwise derivative is circumvented by decoupling the individual equations of the system without a streamwise derivative and solving them separately at each streamwise step of a spatial marching scheme for the remaining equations. However, any severe penalty in economy due to loss of stability in the overall scheme from the decoupling would be unacceptable. The present sequentially

decoupled implicit algorithm decouples the primary/secondary flow equations into subsystems through sequencing and linearization of the subsystems. Each of the subsystems can then be solved by economical, stable, implicit procedures.

3.1 Sequentially Decoupled Implicit Algorithm

The solution algorithm for the primary/secondary flow equations is developed by considering a more general case of a partial differential equation in the form

$$Mq = 0 \tag{3.2}$$

M is a matrix operator (nonlinear) whose elements are the coefficients and differential operators of the individual equations of the system and q is a vector of dependent variables. Further, the elements of q are assumed to be ordered and the sequence of equations in M arranged on the basis of an association between an equation and a dependent variable. This association between individual equations of the system and dependent variables will be clarified with development of the algorithm. The matrix M is decomposed and (3.2) written in the form

$$(L + D + U)q = 0 \tag{3.3}$$

where L, D, U are matrix operators containing the lower diagonal, diagonal and upper diagonal elements of M, respectively. The matrix operators L, D and U are linearized by the following linearization scheme

$$L^{n,n+1} : \ell_{ij}\,(q_k^{n+1},\ q_m^{n}) \qquad \begin{matrix} k = 1, \ldots (j-1) \\ m = j, \ldots N \end{matrix} \tag{3.4}$$

where ℓ_{ij} are the elements of L and n is the marching coordinate index. The operators D and U can be linearized in the same manner as L. Equation (3.3) can be written as a linear, decoupled set of equations

$$(D^{n,n+1} + L^{n,n+1})\ q^{n+1} + U^{n,n+1}\ q^{n} = 0 \tag{3.5}$$

or

$$D^{n,n+1}\, q^{n+1} = -\left(L^{n,n+1}\, q^{n+1} + U^{n,n+1}\, q^{n}\right) \tag{3.6}$$

Equation (3.6) is a decoupled system of equations that can be solved by inverting the linear diagonal operators in sequence using implicit schemes. Clearly, the success of the sequentially decoupled algorithm (3.6) depends on the system of equations (3.2) and the choice of the diagonal matrix operator, D. The diagonal operator, D, is determined by the association made between individual equations of the system and dependent variables.

The association of equations with variables is straightforward for the primary/secondary flow equation; Ω with (2.10), ψ with (2.9), p with (2.11), u_p with (2.8), ϕ with (2.7), and E with (2.12). For simplicity, the implicit operator $(D^{n,n+1} + L^{n,n+1})$ in (3.5) for the incompressible form of the primary/secondary flow equations can be written as

$$\left(D^{n,n+1} + L^{n,n+1}\right) q^{n+1}$$

$$= \begin{bmatrix} d_{11} & * & & * & \\ 1 & \nabla_s^2 & & & \\ \ell_{31} & \ell_{32} & \nabla_s^2 & * & * \\ 0 & 0 & \frac{1}{h}\frac{\partial}{\partial x} & d_{44} & \\ 0 & 0 & 0 & \frac{\partial}{\partial x} & \nabla_s^2 \end{bmatrix} \begin{bmatrix} \Omega \\ \psi \\ p \\ u_p \\ \phi \end{bmatrix}^{n+1} \tag{3.7}$$

where d_{11}, $d_{44} = U\cdot\nabla - Re^{-1}\nabla_s^2$. The '*' in (3.7) is used to indicate non-zero elements of the explicit operator, $U^{n,n+1}$. The vector basis is assumed aligned with coordinate directions in (3.7). The vector basis introduces more complex differential operators in individual equations but the implicit operator retains essentially the same form as (3.7). Although no stability analysis of (3.6) has been performed, stability of (3.6) for the primary/secondary flow

equations has been established through extensive numerical computation of numerous test cases. Further, although the vorticity and vector potential equations (first two equations in (3.7)) can be uncoupled in (3.7), they are strongly coupled at a no-slip boundary by boundary conditions. Consequently, the vorticity and vector potential equations are solved as a coupled subsystem of equations to avoid stability problems. The following sequentially decoupled subsystem equations are obtained for the compressible primary/secondary flow equations

1) vorticity (2.10), vector potential (2.9) for Ω, ψ
2) pressure equation (2.11) for p
3) energy equation (2.12) for E
4) streamwise momentum (2.8) for u_p
5) equation of state (2.13) for ρ (algebraic)
6) scalar potential equation (2.7) for ϕ

The sequence completes the solution of the primary/secondary flow equations for one streamwise step (n+1) from the solution at the previously computed step (n) (initial conditions for n=1). Each of the individual subsystem equations can be solved by a convenient, efficient procedure. Numerical procedures used in the present work for solving decoupled subsystem equations are described in a later section.

3.2 Differencing Procedures and Boundary Conditions

The governing equations (2.7)-(2.12) are transformed to a body-fitted coordinate system in which the equations are discretized. Body-fitted coordinate transformations suitable for the primary/secondary flow equations are discussed in [1]. The discretization employs two-point backward differences for streamwise derivatives and three-point central differences for transverse derivatives. The body-fitted coordinate transformation allows a variable streamwise step size and concentration of grid points in regions of expected large gradients. A centered Crank-Nicolson formulation could be used for streamwise derivatives but the formal accuracy of the scheme would not be improved because of the first-order accurate linearization scheme (3.4) used to decouple subsystem equations.

Implicit boundary conditions are used in all subsystem equations. Boundary conditions that are not straightforward are no-slip conditions on a solid boundary and boundary conditions on pressure. These conditions are described here. The streamwise velocity u_p is specified as zero in the streamwise momentum equation (2.8) on a no-slip boundary. The condition $v = w = 0$ must be expressed in terms of ϕ, ψ and Ω. The normal component of the scalar potential velocity is specified as zero by $\bar{i}_n \cdot \bar{V}_\phi = 0$, where $\bar{i}_n$ is the unit normal vector to the boundary. V_ϕ is specified in terms of ϕ to obtain a Neumann condition for the scalar potential equation (2.7). The normal component of the vector potential velocity is specified zero by prescribing $\psi = 0$ on the boundary. The tangential component of the transverse velocity is specified at the no-slip boundary by

$$\bar{i}_t \cdot [(v_\phi + v_\psi)\bar{e}^2 + (w_\phi + w_\psi)\bar{e}^3] = 0 \qquad (3.8)$$

where $\bar{i}_t$ is the unit tangent vector to the boundary. Equation (3.8) combined with equation (2.9) is used to obtain Ω on the boundary in terms of ϕ and ψ. This relation for Ω, along with prescribing $\psi = 0$, provides coupled boundary conditions for the vector potential (2.9) and vorticity equations (2.10). The coupled boundary conditions require the equations to be solved as a coupled subsystem from stability considerations.

Boundary conditions for pressure are obtained by computing the normal gradient of pressure on the boundary from transverse momentum equations. The prescription of the normal gradient of pressure in the pressure equation (2.11) results in a Neumann problem. Solution of the Neumann problem leaves an undetermined constant in the transverse plane that could, however, be a function of the streamwise coordinate. Pressure, p, is written as

$$p = p_m(x_1) + p_v(x_1, x_2, x_3) \qquad (3.9)$$

where p_m is the undetermined constant of the Neumann problem and p_v is the solution of the pressure equation. The value of p_m is required in the solution of the streamwise momentum equation (2.8) in the form of the streamwise gradient, $\frac{\partial p_m}{\partial x_1}$. In external flows, p_m can be determined by equating

the right-hand side of (3.9) to prescribed pressure at a point in freestream in each transverse plane. Such a condition is not available in internal flows and p_m has to be determined to ensure that the integral mass flux relation

$$\int_A \rho \bar{U} \cdot \bar{i}_1 dA = Q = \text{constant} \qquad (3.10)$$

is satisfied. In the present work, p_m is adjusted by a secant iteration during solution of the streamwise momentum equation (2.8) so that integral mass flux relation (3.10) is satisfied.

3.3 Summary

A summary of the procedure used to advance the solution a single streamwise step to the (n+1) level from previously computed quantities at the n level follows. Coordinate and vector basis information required to solve the primary/secondary equations are prescribed input. Governing equations are assumed to be linearized and discretized as previously described.

(1) Equations (2.9) and (2.10) form a linear coupled system for ψ^{n+1} and Ω^{n+1}, which is solved as a (2×2) coupled system. For this purpose, artificial time derivatives are added to each equation and an iterative block-implicit scheme [2] is used. In prescribing no-slip boundary conditions, the tangential component (3.8) contains a contribution from ϕ; this contribution is evaluated using ϕ^n. Linearization (3.4) provides that terms involving other unknown dependent variables are evaluated at the n-level.

(2) The pressure equation (2.11) is solved for p_v^{n+1} using an iterative scalar ADI scheme. Updated values of v_ψ^{n+1} and w_ψ^{n+1} are available while other dependent variables are evaluated at the n-level.

(3) The energy equation (2.12) is solved for E^{n+1} using a scalar ADI scheme.

(4a) Solution of the streamwise momentum equation is described for internal flow. Using an assumed value of p_m^{n+1} to begin a secant iteration, the streamwise momentum equation (2.8) is solved for u_p^{n+1} using a scalar ADI scheme. The streamwise pressure gradient is evaluated at the (n+1) level.

(4b) The density ρ^{n+1} is evaluated algebraically from the equation of state (2.13)

(4c) The integral mass flux through the transverse plane is computed using (3.10).

(4d) Assuming the initial guess for p_m^{n+1} was not exact, the integral mass flux relation (3.10) will not be satisfied. Steps (4a-c) are repeated iteratively using a standard secant method [3] to find the value of p_m^{n+1} which leads to u_p^{n+1} and ρ^{n+1} satisfying the integral mass flux relation (3.10). In the incompressible limit, all equations in the secant iteration are linear and the third iteration is exact. At high subsonic Mach numbers, a fourth or fifth iteration may be required.

(5) Finally, the scalar potential equation (2.7) is solved for ϕ^{n+1} using an iterative scalar ADI scheme.

REFERENCES

1. Govindan, T.R., Briley, W.R. and McDonald, H.: Generalized Three-Dimensional Viscous Primary/Secondary Flow Equations for Internal and External Flows, Part I - Approximations and Formulation of Equations, SRA Report R87-1 (paper in preparation).

2. Govindan, T.R., Briley, W.R. and McDonald, H.: Generalized Three-Dimensional Viscous Primary/Secondary Flow Equations for Internal and External Flows, Part II - Numerical Solution and Results, Report R87-2 (paper in preparation).

3. Lin, S.J., Levy, R., Shamroth, S.J. and Govindan, T.R.: A Three-Dimensional Viscous Flow Analysis for the Helicopter Tip Vortex Generation Problem, NASA CR 3906, 1985.

4. De Jong, F.J., Govindan, T.R., Levy, R. and Shamroth, S.J.: Validation of a Forward-Marching Procedure to Compute the Tip Vortex Generation Process for Ship Propeller Blades, presented at the 17th Symposium on Naval Hydrodynamics, The Hague, The Netherlands, 1988.

5. Briley, W.R. and McDonald, H.: On the Structure and Use of Linearized Block Implicit Schemes, Journal of Comp. Physics, Vol. 34, No. 1, pp. 54-72, January 1980.

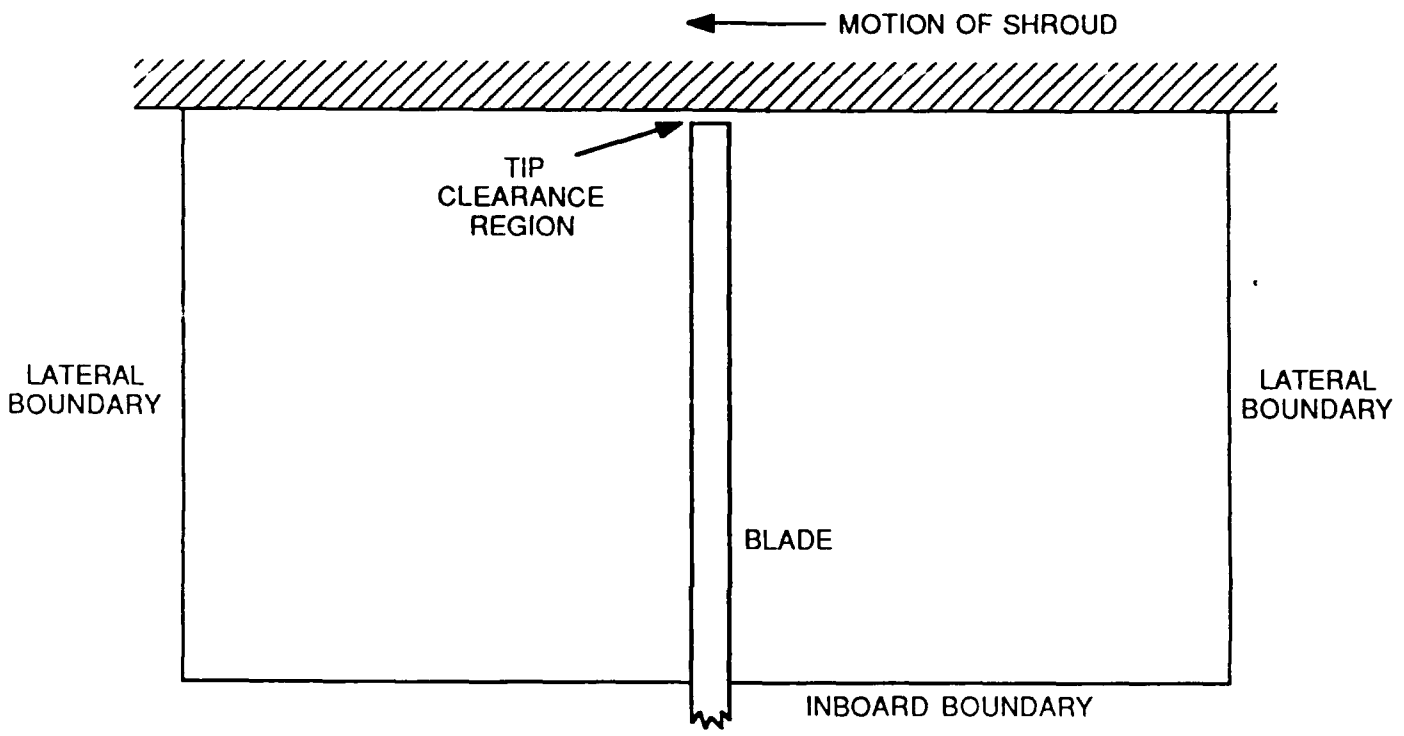

TIP CLEARANCE GAP = 0.01 CHORD

INBOARD AND LATERAL BOUNDARIES ARE 0.5 CHORDS FROM TIP

Re = 20,000 (LAMINAR FLOW)

SHROUD VELOCITY = 0.5 PRIMARY FLOW VELOCITY

Figure A. Schematic of Cross-Section Normal to Primary Flow Direction for Shrouded Tip Flow Application.

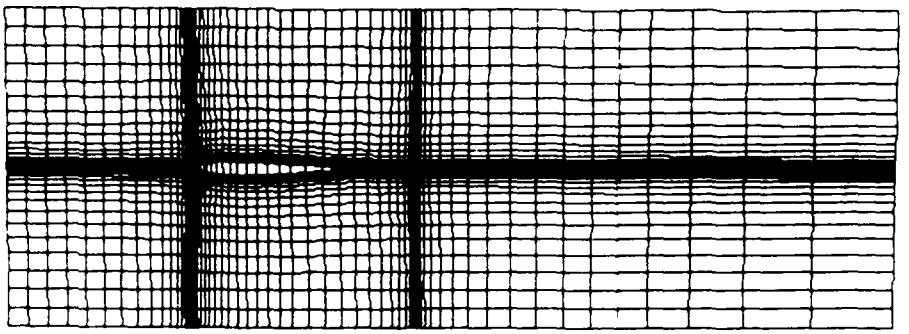

Figure 1a. Single Airfoil.

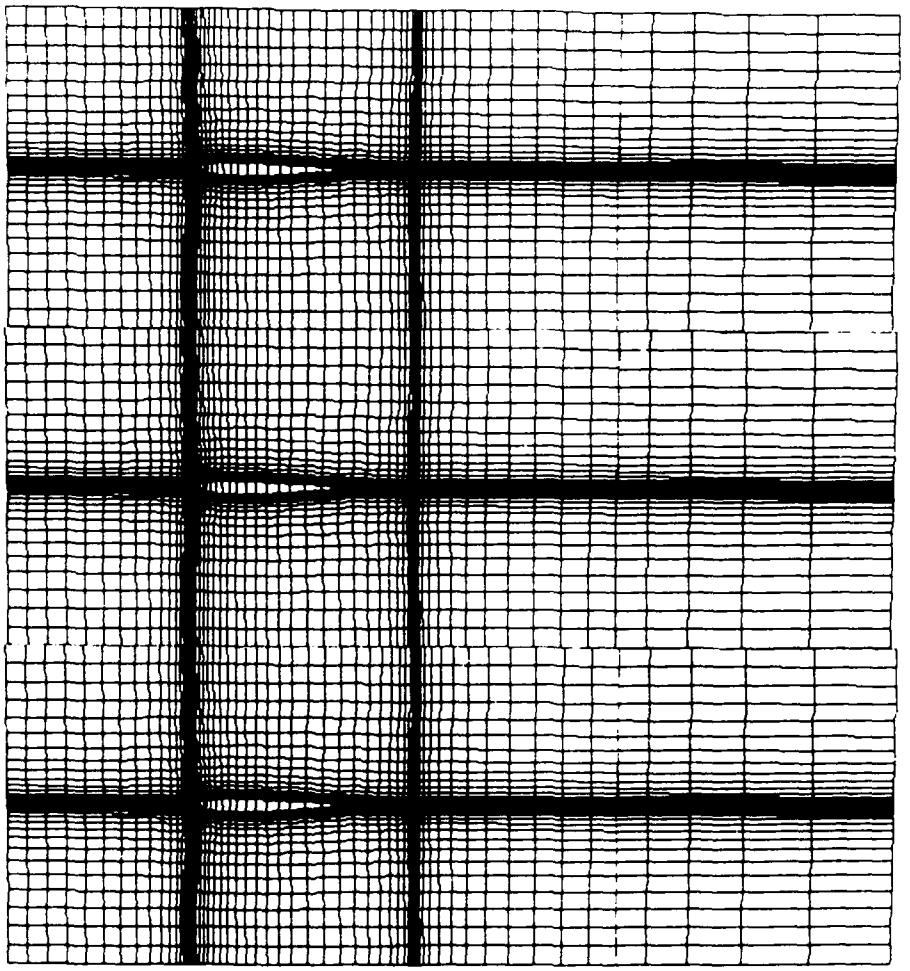

Figure 1b. Zero Pitch Planar Cascade.

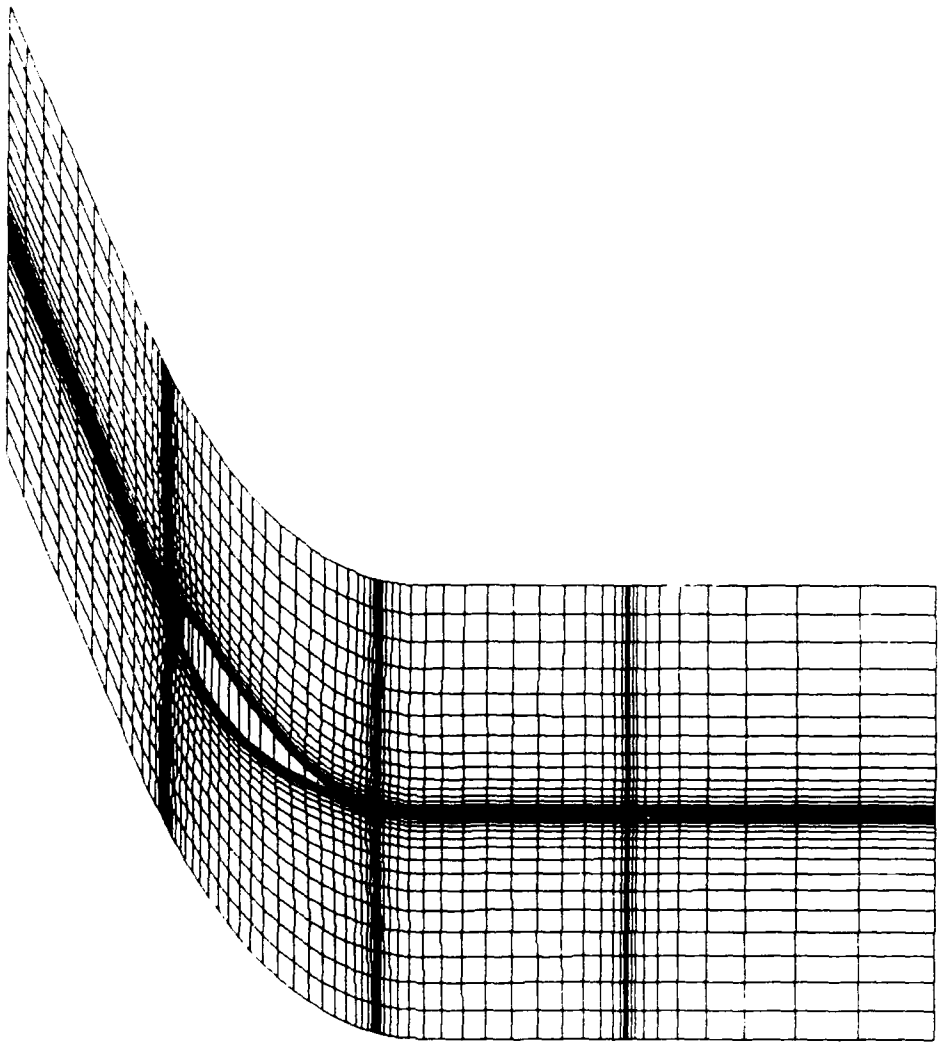

Figure 2. Sheared Airfoil Coordinates Blade, Thickness from Eq. 1.

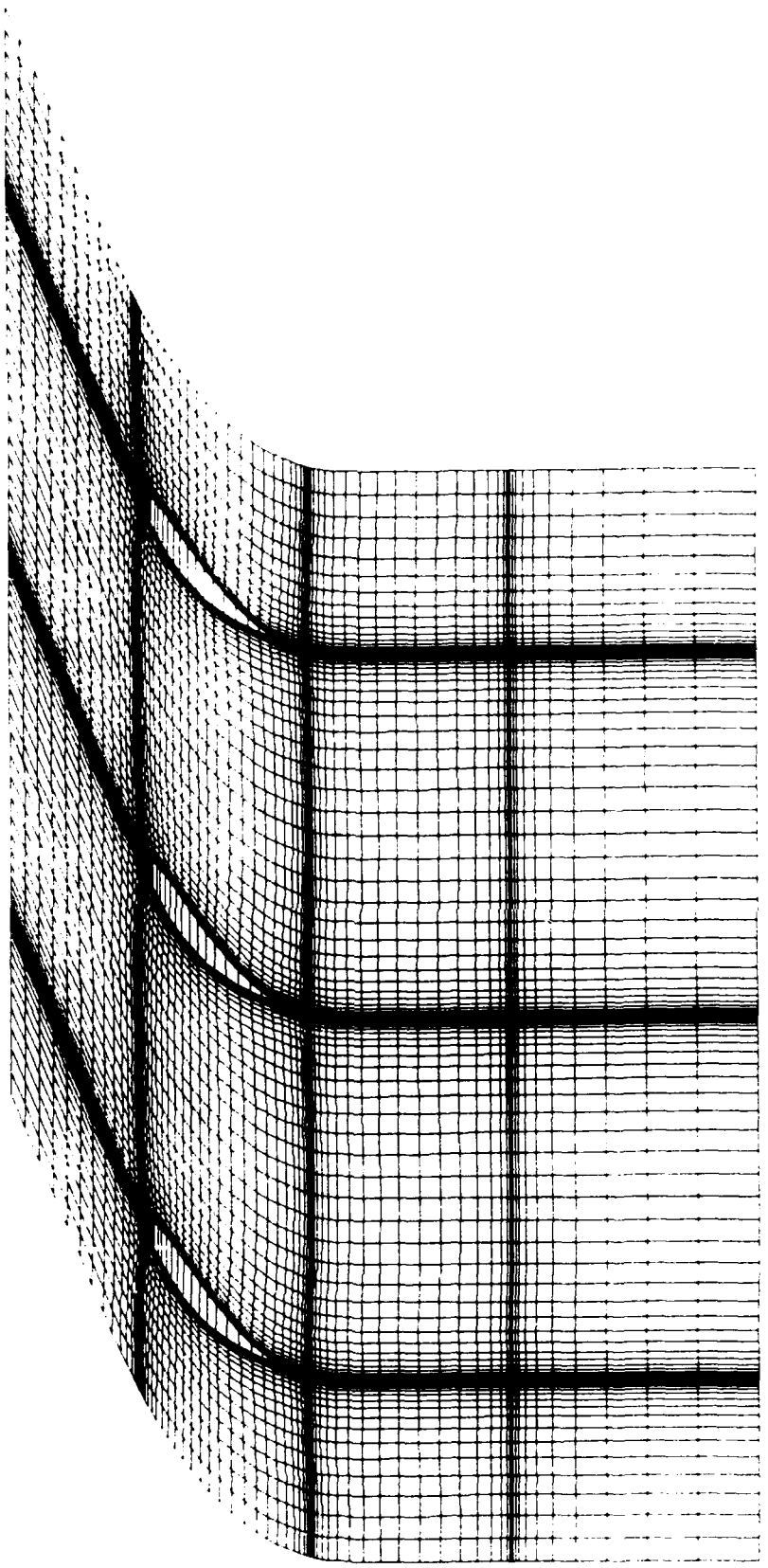

Figure 3. Planar Cascade of Airfoils.

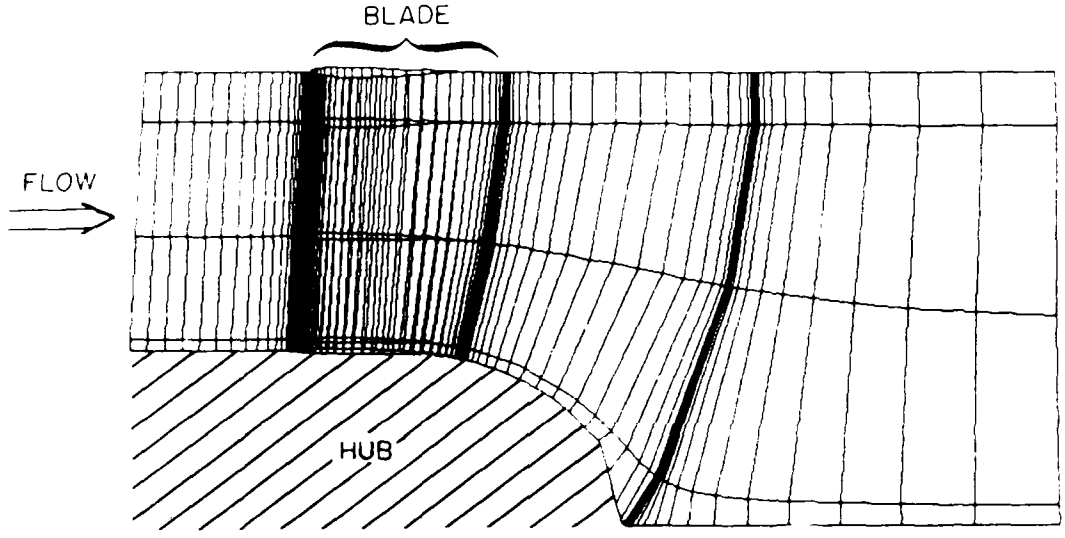

Figure 4. R,Z Coordinate Surface (Side View).

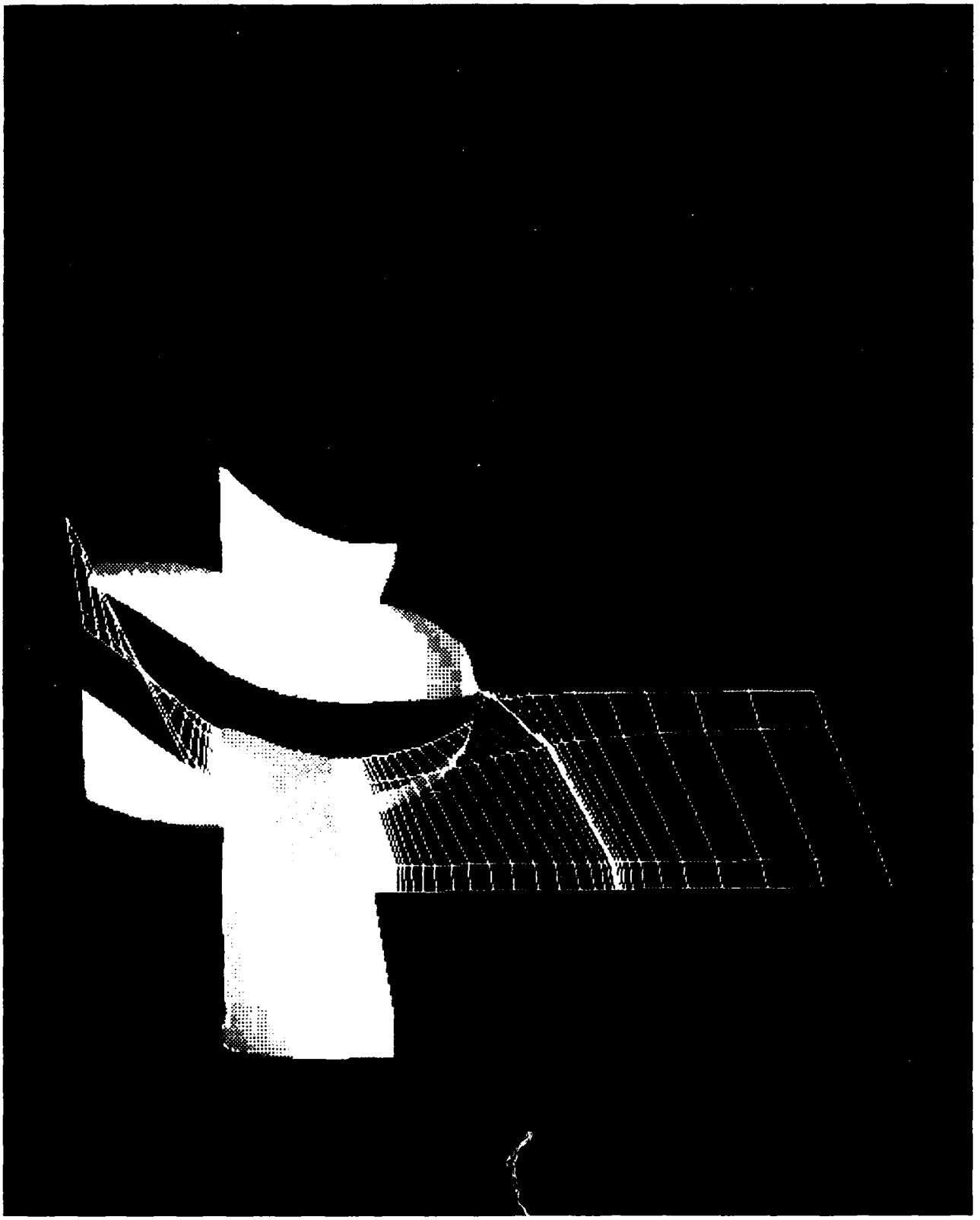

Figure 5. Top View of Lab showing R,Z coordinates in Units.

Figure 6. Hub and Shroud Coordinate Surfaces with Three Blades.